Journal of Applied Science and Engineering, Vol. 16, No. 2, pp. 117–126 (2013) *DOI: 10.6180/jase.2013.16.2.02*

Equipment Fragility Caused by Shock Excitations

Alexander Y. Tuan[1]* and Chun Kuang Chen[1,2]

[1]*Department of Civil Engineering, Tamkang University, Tamsui, Taiwan 251, R.O.C.*
[2]*Pacific Engineers & Constructors, Ltd.*

Abstract

Due to its simplicity, shock response spectrum has become widely used as a means of describing the shock responses and fragilities of structures and equipment. This study focuses on the drawbacks of using shock excitation response spectrum for defining equipment shock tolerance. A cantilever beam with a tip mass was used to model a hypothetical equipment, subjected to strong ground motion such as that due to an explosion or a sudden excitation. The exact solution from a detailed modal analysis shows that multiple modes of response were excited. Contributions from higher modes can be more predominant than that from the fundamental mode. Assuming that the total response of the equipment is predominantly in the first mode is erroneous. Current procedures for equipment fragility tests are inadequate, not only due to physical limitations of shake table tests, but also due to the lack of a reliable analytical model.

Key Words: Equipment, Fragility, Shock Response Spectrum, Modal Analysis, Spectral Analysis, Fast Fourier Transform

1. Introduction

The shock response of equipment is often represented by a shock response spectrum (SRS), which is the envelope of the maximum responses of a damped single-degree-of-freedom (SDOF) oscillator subjected to support excitations over a specified frequency range. Due to its simplicity, SRS has become widely employed as a means of describing the shock responses and fragilities of structures [1–9] and equipment [10–15]. However, this widely used method has encountered some insufficiency under certain circumstances. This study focuses on the drawbacks of using shock response spectrum for defining equipment shock tolerance. Several papers, majorly consider structures, have already pointed out the shortcomings of using a design response spectrum due to multi-dimensional motion and the combinatorial methodologies for inclusion of higher modes [16,17] and nonlinear responses [18]. This paper illustrates, using a cantilever beam with a tip mass equipment model, that a strong ground shock such as due to an explosion or a sudden excitation can generate multiple modes of responses; therefore, assuming that the total response of the equipment is predominated by the first mode could be erroneous. Besides, current procedures for equipment fragility tests are inadequate, not only due to physical limitations of shake table tests, but also due to the lack of an analytical model.

*Corresponding author. E-mail: alextuan@tku.edu.tw

2. Equipment Fragility

A fragility envelope displays equipment's capacity to resist transient support motion in terms of motion amplitude versus frequency. Therefore, it is essentially a response spectrum at which equipment failure occurs. Equipment failure is usually defined as mechanical damage or loss of function. Expressing equipment fragility in terms of shock response spectra greatly simplifies the design of equipment shock isolation. However, the applicability of a design shock spectrum is often questionable.

The approach commonly employed to determine equipment fragility is to physically test an equipment

item on a shake table of a certain intensity and frequency. Failure modes of equipment may be related to amplitudes and frequencies of the motions at various locations on the equipment. An Equipment Fragility and Protection Procedure was developed by Wilcoski et al. [11] to determine if equipment is vulnerable to prescribed support motions. The purpose of the procedure is to determine the levels of motion at which equipment fails across a broad frequency range. The fragility data was presented in terms of support motion spectral amplitude or response spectral amplitude. The procedure defines the frequency range at which the equipment is vulnerable and the mode or modes of failure. The fragility data reported therein may be used to develop methods of protecting equipment, either by strengthening or isolation of the equipment.

During the development of the procedure, fragility data was gathered based on shake table tests. A random signal is passed through high- and low-pass filters to drive the shake table. This process creates a random motion with the energy of the motion concentrated within a narrow frequency band, and the center frequency moves at a given sweep rate (e.g., the center frequency is doubled every 5 seconds). The intensity of the base motion is progressively increased until failure occurs. Inevitably, the frequency range of the shake table motion is physically limited. Nevertheless, equipment is vulnerable to low frequency amplitudes and is unlikely to fail at very high frequencies. For instance, desktop computers were most vulnerable to failure at frequencies above 15 Hz. However, for shock-induced base motion, equipment modal responses associated with higher frequency range may be significant, as will be illustrated in an example in this paper. The shock response spectrum of the base motion which causes the equipment to fail is called the fragility spectrum of the equipment. By comparing the fragility spectrum of an equipment item to the design shock response spectrum at the proposed equipment location, shock isolation requirements can be easily assessed.

3. Limitations of the Shock Response Spectrum (SRS) Approach

Using shock spectra for equipment fragility assessment is oversimplified, and the approach ignores several sources of error. The most important source of error is the fact that an SRS does not correspond to a unique input time-history. An infinite number of different base motions can generate a given SRS. These different base motions could vary greatly in duration, frequency content and amplitude. The main assumption behind the SRS approach to equipment fragility is that equipment failure is independent of the input waveform. All input base motions corresponding to the SRS are assumed to result in the same failure mode. The possibility of a single item of equipment possessing multiple failure modes is generally not considered. In reality, equipment fragility spectra are only valid for frequencies close to the natural frequencies at which the equipment was actually tested. Extrapolating equipment fragility based on existing databases such as shipboard testing data [19] to the shock environment due to explosion is questionable but routinely done. The validity of this extrapolation has not been verified. Equipment qualification methods are often based on either response spectra or power spectral density (PSD) of support acceleration that does not provide information on the specific frequency of motions that caused failures. Further, a base motion is generally three-dimensional and the peak response amplitude may be quite different from that of unidirectional base motion.

Years of earthquake engineering research have shown that all earthquake response spectra display similar characteristics. Approximate upper bound response spectra may be constructed, based only on the peak displacement, velocity and acceleration of the oscillator base. Kiger et al. [20] have shown that in-structure shock response spectra can be bounded by multiplying the peak in-structure displacement, velocity and acceleration by factors of 1.2, 1.5 and 2.0, respectively. Shock response spectra generated by this technique are assumed to give an upper bound on the response of an oscillator, with 5 to 10 percent of critical damping, located near the center of a buried facility. Approximate shock response spectra generated by this approach are assumed to represent the upper bound of the actual shock response spectra and independent of the precise form of the input motion. Since in-structure motions are typically described using tripartite shock response spectra, it was only natural to attempt to quantify equipment failure in terms of shock spectra.

4. Fragility Spectrum of an Ideal Equipment

To illustrate the limitations of using SRS for fragility assessment, a cantilever beam, carrying a tip mass having both translational and rotary inertia, was used as

"ideal" equipment subject to a series of simulated shock testing. The equipment response was assumed to be linearly elastic. The mass density, cross-sectional area, Young's modulus, moment of inertia and length of the beam are denoted by ρ, A, E, I and L, respectively. These parameters were assumed constant along the beam. The mass and the radius of gyration of the tip mass are denoted by m and r, respectively. This simple equipment model is shown in Figure 1. Exact solutions of the structural response $u(x, t)$ can be obtained by modal analysis if the support motion can be expressed in terms of a simple analytical function.

The equation of motion along with the initial and boundary conditions for this structural system subjected to a support motion is derived herein. The support motion is prescribed as an acceleration time-history, $\ddot{u}_g(t)$. The relative displacement of the beam with respect to the support is denoted as $u(x, t)$. From Figure 1, the total beam deflection is

$$y(x,t) = u(x,t) + u_g(t) \tag{1}$$

where $u(x, t)$ is the beam deflection with respect to the support, and $u_g(t)$ is the support movement.

4.1 Governing Equation

The equation of motion for a differential beam element is

$$-\frac{\partial V}{\partial x}dx = \rho A dx \frac{\partial^2 y}{\partial t^2} = \rho A dx \frac{\partial^2}{\partial t^2}(u + u_g) \tag{2}$$

The shear force in the beam, V, is usually expressed as the moment gradient:

$$V = \frac{\partial M}{\partial x} \tag{3}$$

The beam moment-curvature relation is

$$M = EI\frac{\partial^2 u}{\partial x^2} \tag{4}$$

Substituting Eqs. (3) and (4) into Eq. (2) yields

$$-EI\frac{\partial^4 u}{\partial x^4} = \rho A\frac{\partial^2 u}{\partial t^2} + \rho A\frac{\partial^2 u_g}{\partial t^2} \tag{5}$$

or, alternatively,

$$\frac{\partial^4 u}{\partial x^4} + \frac{\rho A}{EI}\frac{\partial^2 u}{\partial t^2} = -\frac{\rho A}{EI}\frac{\partial^2 u_g}{\partial t^2} \tag{6}$$

The initial conditions are assumed to be at rest,

$$y(x,0) = 0 \quad (0 \le x \le L) \tag{7}$$

and

$$\frac{\partial y}{\partial t}(x,0) = 0 \quad (0 \le x \le L) \tag{8}$$

The boundary conditions at the fixed end are

$$u(0,t) = 0 \quad (t \ge 0) \tag{9}$$

and

$$\frac{\partial u}{\partial x}(0,t) = 0 \quad (t \ge 0) \tag{10}$$

The boundary conditions at the end attached to the tip mass are

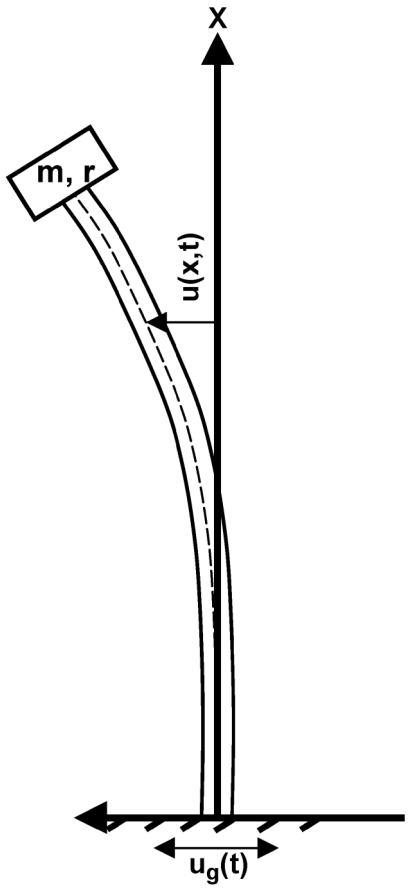

Figure 1. Cantilever beam carrying a tip mass with translational and rotary inertia.

$$EI\frac{\partial^2 u}{\partial x^2}(L,t) = -mr^2\frac{\partial^2}{\partial t^2}\left[\frac{\partial u}{\partial x}(L,t)\right] \quad (t \geq 0) \tag{11}$$

and

$$EI\frac{\partial^3 u}{\partial x^3}(L,t) = m\frac{\partial^2 y}{\partial t^2}(L,t) \quad (t \geq 0) \tag{12}$$

where Eqs. (11) and (12) represent the moment and shear equilibrium conditions at the tip mass, respectively.

4.2 Closed-form Solution

Let

$$\alpha = \frac{u}{L} \tag{13}$$

$$\beta = \frac{u_g}{L} \tag{14}$$

$$\xi = \frac{x}{L} \tag{15}$$

and Eq. (6) can be rewritten as

$$\frac{\partial^4\alpha}{\partial\xi^4} + \frac{\rho AL^4}{EI}\frac{\partial^2\alpha}{\partial t^2} = \frac{\rho AL^4}{EI}\frac{\partial^2\beta}{\partial t^2} \tag{16}$$

where the negative sign of the support motion is dropped. Introducing

$$T = L^2\sqrt{\frac{\rho A}{EI}} \tag{17}$$

and

$$\psi = \frac{t}{T} \tag{18}$$

and Eq. (16) can be written in the dimensionless form:

$$\frac{\partial^4\alpha}{\partial\xi^4} + \frac{\partial^2\alpha}{\partial\psi^2} = \frac{\partial^2\beta}{\partial\psi^2} \tag{19}$$

with the corresponding initial and boundary conditions:

$$\alpha(\xi,0) = 0 \quad (0 \leq \xi \leq 1) \tag{20}$$

$$\frac{\partial\alpha}{\partial\psi}(\xi,0) = 0 \quad (0 \leq \xi \leq 1) \tag{21}$$

$$\alpha(0,\psi) = 0 \quad (\psi \geq 0) \tag{22}$$

$$\frac{\partial\alpha}{\partial\xi}(0,\psi) = 0 \quad (\psi \geq 0) \tag{23}$$

$$\frac{\partial^2\alpha}{\partial\xi^2}(1,\psi) = -\frac{mr^2}{\rho AL^3}\left[\frac{\partial^3\alpha}{\partial\xi\partial\psi^2}(1,\psi)\right] \quad (\psi \geq 0) \tag{24}$$

$$\frac{\partial^3\alpha}{\partial\xi^3}(1,\psi) = \frac{m}{\rho AL}\left[\frac{\partial^2\alpha}{\partial\psi^2}(1,\psi) + \frac{\partial^2\beta}{\partial\psi^2}(\psi)\right] \quad (\psi \geq 0) \tag{25}$$

The natural frequencies and mode shapes can be obtained from the homogeneous part of Eq. (19),

$$\frac{\partial^4\alpha}{\partial\xi^4} + \frac{\partial^2\alpha}{\partial\psi^2} = 0 \tag{26}$$

Solving it by method of separation of variables,

$$\alpha(\xi,\psi) = \phi(\xi)\theta(\psi) \tag{27}$$

and using

$$\phi' = \frac{d\phi}{d\xi} \text{ and } \dot{\theta} = \frac{d\theta}{d\psi} \tag{28}$$

Eq. (26) can be written as

$$\frac{\phi^{IV}}{\phi} + \frac{\ddot{\theta}}{\theta} = 0 \tag{29}$$

and both terms must be a constant, that is,

$$\frac{\phi^{IV}}{\phi} = -\frac{\ddot{\theta}}{\theta} = \lambda^4 \tag{30}$$

The solution of ϕ takes the following form

$$\phi = Af_1 + Bf_2 + Cf_3 + Df_4 \tag{31}$$

where

$$f_1 = \cosh\lambda\xi + \cos\lambda\xi \tag{32}$$

$$f_2 = \sinh\lambda\xi - \sin\lambda\xi \tag{33}$$

$$f_3 = \cosh\lambda\xi - \cos\lambda\xi \tag{34}$$

$$f_4 = \sinh\lambda\xi + \sin\lambda\xi \tag{35}$$

Since $f_1(0) = 2$, $f_2(0) = f_3(0) = f_4(0) = 0$, Eqs. (22) and (31) yield $\phi(0) = 2A = 0$ and Eqs. (23) and (28) yield $\phi'(0) = 2\lambda D = 0$. Therefore, $A = D = 0$.

Let

$$f_i(1) = F_i, \ i = 1, \ 2, \ 3 \text{ and } 4 \tag{36}$$

$$\frac{m}{\rho AL} = k_1 \tag{37}$$

$$\left(\frac{r}{L}\right)^2 = k_2 \tag{38}$$

then Eqs. (24), (28) and (31) yield

$$\phi''(1)\theta = -k_1 k_2 \phi'(1)\ddot{\theta} \tag{39}$$

or

$$B(F_4 - k_1 k_2 \lambda^3 F_3) + C(F_1 - k_1 k_2 \lambda^3 F_4) = 0 \tag{40}$$

and Eqs. (25), (28) and (31) yield

$$\phi'''(1)\theta = k_1 \phi(1)\ddot{\theta} \tag{41}$$

or

$$B(F_1 + k_1 \lambda F_2) + C(F_2 + k_1 \lambda F_3) = 0 \tag{42}$$

Eqs. (40) and (42) give relative values of B and C

$$\frac{C}{B} = -\frac{F_4 - k_1 k_2 \lambda^3 F_3}{F_1 - k_1 k_2 \lambda^3 F_4} = -\frac{F_1 + k_1 \lambda F_2}{F_2 + k_1 \lambda F_3} = \gamma \tag{43}$$

A "characteristic equation" can be written as

$$(F_2 + k_1 \lambda F_3)(F_4 - k_1 k_2 \lambda^3 F_3) - (F_1 + k_1 \lambda F_2)(F_1 - k_1 k_2 \lambda^3 F_4) = 0 \tag{44}$$

and each root of Eq. (44), λ_i, is called a "characteristic value."

For each λ_i, there is a corresponding ratio given by Eq. (43)

$$\gamma_i = \frac{C_i}{B_i} \tag{45}$$

which is used to determine the relative coefficients in the i^{th} mode shape given by Eq. (31).

From Eqs. (16) and (30), it can be shown that solution of θ yields the natural circular frequencies, ω_n, which are related to the characteristic values λ_n by

$$\omega_n^2 = \frac{\lambda_n^4 EI}{\rho A L^4} \tag{46}$$

and the natural cyclic frequencies can be expressed as

$$f_n = \frac{\lambda_n^2}{2\pi T} \tag{47}$$

where n denotes the mode number.

If the structural response under support motion is linearly elastic, the total beam deflection $y(x, t)$ can be expressed as the sum of modal contributions.

4.3 Modal Equations of Motion by Hamilton's Principle

Due to orthogonality of vibration modes, each modal equation of motion can be solved separately as that for a SDOF system. Based on the principle of linear superposition, the total response of the system can be expressed as the sum of modal contributions. The beam deflection $u(x, t)$ can be expressed in terms of relative modal amplitudes q_i and shapes η_i as

$$u(x,t) = \sum_{i=1}^{\infty} q_i(t)\eta_i(x) \tag{48}$$

and then

$$y(x,t) = \sum_{i=1}^{\infty} q_i(t)\eta_i(x) + u_g(t) \tag{49}$$

The kinetic energy of the system is

$$\Omega = \frac{1}{2}\int_0^L \rho A\left(\frac{\partial y}{\partial t}\right)^2 dx + \frac{1}{2}m\left(\frac{\partial y}{\partial t}\right)^2_{x=L} + \frac{1}{2}mr^2\left(\frac{\partial^2 y}{\partial x \partial t}\right)^2_{x=L} \tag{50}$$

and the strain energy of the system is

$$U = \frac{1}{2}\int_0^L EI\left(\frac{\partial^2 u}{\partial x^2}\right)^2 dx \tag{51}$$

Applying Hamilton's Principle,

$$\int_{t_1}^{t_2} \delta(\Omega - U)dt = 0 \tag{52}$$

where

$$\delta\Omega = \int_0^L \rho A\dot{y}\delta\dot{y}dx + m\dot{y}_L\delta\dot{y}_L + mr^2\dot{u}'_L\delta\dot{u}'_L \tag{53}$$

and

$$\delta U = \int_0^L EIu''\delta u''dx \tag{54}$$

Using the following expressions,

$$\dot{y} = \sum_{i=1}^{\infty}\dot{q}_i\eta_i + \dot{u}_g \tag{55}$$

$$\delta\dot{y} = \delta\dot{u} = \sum_{i=1}^{\infty}\delta\dot{q}_i\eta_i \tag{56}$$

$$\dot{y}_L = \dot{u}_L + \dot{u}_g = \sum_{i=1}^{\infty} \dot{q}_i \eta_i(L) + \dot{u}_g \tag{57}$$

$$\delta\dot{y}_L = \delta\dot{u}_L = \sum_{i=1}^{\infty} \delta\dot{q}_i \eta_i(L) \tag{58}$$

$$u' = \sum_{i=1}^{\infty} q_i \eta_i' \tag{59}$$

$$\dot{u}' = \sum_{i=1}^{\infty} \dot{q}_i \eta_i' \tag{60}$$

$$\dot{u}_L' = \sum_{i=1}^{\infty} \dot{q}_i \eta_i'(L) \tag{61}$$

$$\delta\dot{u}_L' = \sum_{i=1}^{\infty} \delta\dot{q}_i \eta_i'(L) \tag{62}$$

$$u'' = \sum_{i=1}^{\infty} q_i \eta_i'' \tag{63}$$

$$\delta u'' = \sum_{i=1}^{\infty} \delta q_i \eta_i'' \tag{64}$$

Eq. (52) can be written as

$$\begin{aligned}&\int_{t_1}^{t_2}\Bigg[\int_0^L \rho A\left(\sum \dot{q}\eta + \dot{u}_g\right)\left(\sum \delta\dot{q}\eta\right)dx \\ &+ m\left(\sum \dot{q}\eta(L) + \dot{u}_g\right)\left(\sum \delta\dot{q}\eta(L)\right) \\ &+ mr^2\left(\sum \dot{q}\eta'(L)\right)\left(\sum \delta\dot{q}\eta'(L)\right) \\ &- \int_0^L EI\left(\sum q\eta''\right)\left(\sum \delta q\eta''\right)dx\Bigg]dt = 0\end{aligned} \tag{65}$$

$$\begin{aligned}&\int_0^L \rho A\left(\sum \dot{q}\eta + \dot{u}_g\right)\left(\sum \delta\dot{q}\eta\right)dx = \sum_{i=1}^{\infty}\sum_{j=1}^{\infty} \dot{q}_i \delta\dot{q}_j \int_0^L \rho A\eta_i\eta_j dx \\ &+ \dot{u}_g \sum_{i=1}^{\infty} \delta\dot{q}_i \int_0^L \rho A\eta_i dx\end{aligned} \tag{66}$$

$$\begin{aligned}&m\left(\sum \dot{q}\eta(L) + \dot{u}_g\right)\left(\sum \delta\dot{q}\eta(L)\right) \\ &= m\sum_{i=1}^{\infty}\sum_{j=1}^{\infty} \dot{q}_i \delta\dot{q}_j \eta_i(L)\eta_j(L) + m\dot{u}_g \sum_{i=1}^{\infty} \delta\dot{q}_i \eta_i(L)\end{aligned} \tag{67}$$

$$mr^2\left(\sum \dot{q}\eta'(L)\right)\left(\sum \delta\dot{q}\eta'(L)\right) = mr^2 \sum_{i=1}^{\infty}\sum_{j=1}^{\infty} \dot{q}_i \delta\dot{q}_j \eta_i'(L)\eta_j'(L) \tag{68}$$

$$\int_0^L EI\left(\sum q\eta''\right)\left(\sum \delta q\eta''\right)dx \sum_{i=1}^{\infty}\sum_{j=1}^{\infty} q_i \delta q_j \int_0^L EI\eta_i''\eta_j'' dx \tag{69}$$

Integrating Eq. (65) by parts and using Eqs. (66) through (69),

$$\begin{aligned}&\sum_{i=1}^{\infty}\sum_{j=1}^{\infty}\left(\int_0^L \rho A\eta_i\eta_j dx \dot{q}_i\, \delta q_j\Big|_{t_1}^{t_2} - \int_{t_1}^{t_2} \ddot{q}_i \delta q_j \int_0^L \rho A\eta_i\eta_j dx dt\right) \\ &+ \sum_{i=1}^{\infty}\left(\dot{u}_g \int_0^L \rho A\eta_i dx\, \delta q_i\Big|_{t_1}^{t_2} - \int_{t_1}^{t_2} \ddot{u}_g \delta q_i \int_0^L \rho A\eta_i dx dt\right) \\ &+ m\sum_{i=1}^{\infty}\sum_{j=1}^{\infty}\left(\eta_i(L)\eta_j(L)\dot{q}_i\, \delta q_j\Big|_{t_1}^{t_2} - \int_{t_1}^{t_2} \ddot{q}_i \delta q_j \eta_i(L)\eta_j(L) dt\right) \\ &+ m\sum_{i=1}^{\infty}\left(\dot{u}_g \eta_i(L)\delta q_i\Big|_{t_1}^{t_2} - \int_{t_1}^{t_2} \ddot{u}_g \delta q_i \eta_i(L) dt\right) \\ &+ mr^2\sum_{i=1}^{\infty}\sum_{j=1}^{\infty}\left(\eta_i'(L)\eta_j'(L)\dot{q}_i\, \delta q_j\Big|_{t_1}^{t_2} - \int_{t_1}^{t_2} \ddot{q}_i \delta q_j \eta_i'(L)\eta_j'(L) dt\right) \\ &- \sum_{i=1}^{\infty}\sum_{j=1}^{\infty}\int_{t_1}^{t_2} q_i \delta q_j \int_0^L EI\eta_i''\eta_j'' dx dt = 0\end{aligned} \tag{70}$$

Rearranging terms yields

$$\begin{aligned}&\sum_{i=1}^{\infty}\sum_{j=1}^{\infty}\int_{t_1}^{t_2}\Bigg\{\ddot{q}_i\left[\int_0^L \rho A\eta_i\eta_j dx + m\eta_i(L)\eta_j(L) + mr^2\eta_i'(L)\eta_j'(L)\right] \\ &+ q_i \int_0^L EI\eta_i''\eta_j'' dx\Bigg\}\delta q_j dt = -\sum_{i=1}^{\infty}\int_{t_1}^{t_2} \ddot{u}_g\left[\int_0^L \rho A\eta_i dx + m\eta_i(L)\right]\delta q_i dt\end{aligned} \tag{71}$$

It can be shown based on the orthogonality of mode shapes that

$$\int_0^L \rho A\eta_i\eta_j dx + m\eta_i(L)\eta_j(L) + mr^2\eta_i'(L)\eta_j'(L) = c_i\overline{\delta_{ij}} \tag{72}$$

where $c_i = \int_0^L \rho A\eta_i^2 dx + m\eta_i(L)^2 + mr^2\eta_i'(L)^2$ and $\overline{\delta_{ij}} = 1$ if $i = j$ and $\overline{\delta_{ij}} = 0$ if $i \neq j$.

Furthermore,

$$\begin{aligned}&\int_0^L EI\eta_i''\eta_j'' dx = 0 \qquad \text{for } i \neq j \\ &\qquad = \frac{EI}{L^3}\lambda_i^4 \quad \text{for } i = j\end{aligned} \tag{73}$$

Substituting Eqs. (72) and (73) into Eq. (71),

$$\int_{t_1}^{t_2}\sum_{i=1}^{\infty}\left(c_i\ddot{q}_i + \frac{EI}{L^3}\lambda_i^4 q_i + \ddot{u}_g\left[\int_0^L \rho A\eta_i dx + m\eta_i(L)\right]\right)\delta q_i dt = 0 \tag{74}$$

Since δq_i are arbitrary variations, it is necessary that

$$\ddot{q}_i + \frac{EI}{L^3}\lambda_i^4 q_i = -\ddot{u}_g \left[\int_0^L \rho A \eta_i dx + m\eta_i(L) \right] / c_i \tag{75}$$

for all i's. Eq. (75) is the equation of motion for mode i and its non-dimensional form can be expressed as

$$\ddot{\theta}_i + \frac{\lambda_i^4}{T}\theta_i = -\ddot{\beta}\left[\int_0^1 \phi_i d\xi + k_1 \phi_i(1) \right] \tag{76}$$

where the sum of the terms in the bracket is the "effective modal mass."

5. Numerical Simulation of Fragility Experiment

The shock response of a hypothetical piece of equipment is assumed to be "perfectly" represented by the cantilever beam with a tip mass model. The parameters of the model are given in Table 1. Based on Eqs. (17), (37) and (38), the characteristic period of the system, T = 0.02 s, along with $k_1 = 1$ and $k_2 = 0.0025$, is used for this example. The characteristic curve (i.e., the plot of Eq. (44)) of this system is shown in Figure 2. The roots of this curve are the characteristic values of the free-vibration equation (Eq. (26)) and the corresponding characteristic functions (obtained from Eqs. (31) and (43)) are the free-vibration mode shapes. Although there are infinite numbers of natural vibration modes existing in this system, only the first seven modes are retained for a modal analysis. The characteristic values of these modes are identified in Table 2. The normalized shapes of the first seven modes are shown in Figure 3. The accuracy of the characteristic values and mode shapes deteriorates with higher modes, though the contributions from higher modes are relatively insignificant.

The base acceleration expression can be derived from Eq. (14) as

$$\ddot{u}_g(t) = \frac{d^2 u_g}{dt^2} = \frac{L}{T^2}\ddot{\beta}(\psi) \tag{77}$$

A unit triangular pulse with duration t_d and no rise time was used to simulate the support motion (or base acceleration) due to an explosion. Mathematically, the base acceleration can be expressed as

$$\ddot{\beta}(\psi) = 1 - \frac{\psi}{t_d / T} \tag{78}$$

Let

Table 1. Parameters of a cantilever beam with a tip mass model

Model Parameter	Value
Length, L (in.)	36
Cross-sectional Area, A (in.^{2})	10
Mass Density, ρ (lb/in.^{3})	7.226×10^{-3}
Tip Mass, m (lb)	2.602
Radius of Gyration, r (in.)	1.8
Young's Modulus, E (psi)	4×10^6
Moment of Inertia, I (in.^{4})	2.36

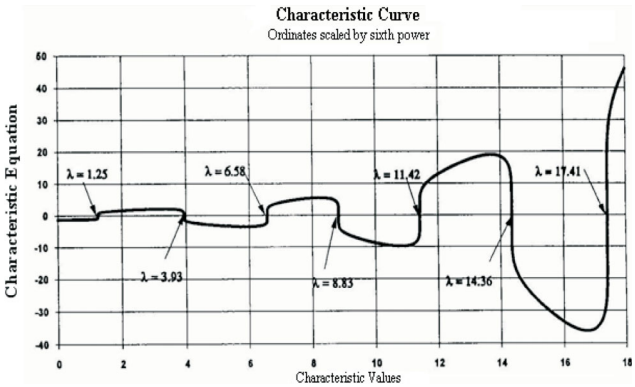

Figure 2. Characteristic curve.

Table 2. Modal properties

Mode No.	Characteristic value	Cyclic Frequency, f_n (Hz)	Effective mass
1	1.247	12.37	0.976
2	3.928	122.78	0.471
3	6.577	344.23	0.254
4	8.832	620.74	0.186
5	11.417	1037.28	0.162
6	14.355	1639.82	0.135
7	17.414	2413.17	0.057

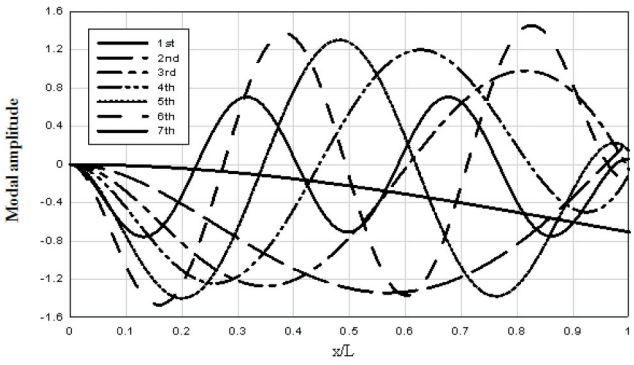

Figure 3. Mode shapes of the cantilever beam with a tip mass.

$$a^2 = \frac{\lambda^4}{T} \text{ and } K = \int_0^1 \phi_i d\xi + k_1 \phi_i(1) \quad (79)$$

the exact solution to Eq. (76) can be expressed as

$$\theta(\psi) = \frac{K}{a^2}\cos(a\psi) - \frac{K}{a^3(t_d/T)}\sin(a\psi) - \frac{K}{a^2}\left(1 - \frac{\psi}{t_d/T}\right) \quad (80)$$
$$0 \le \psi \le t_d/T$$

A free vibration ensues at the end of the triangular pulse. In the example, the pulse duration is varied at t_d/T = 0.1, 0.5, 1, 2 and 5, as shown in Figure 4. The frequency contents of these triangular pulses are presented in Figure 5, by fast Fourier transform (FFT). It can be seen that the shorter the pulse duration, the higher is the frequency contents. However, the energy level is lower for shorter pulses. The equipment response is assumed to be represented by the first seven modes, covering a response frequency range between 0 and 2500 Hz.

The effects of the pulse duration on the equipment response parameters, such as the tip mass displacement, base shear and base moment, were evaluated for the various t_d/T. The analysis results are presented in Table 3. A typical time-history of the base shear and the corresponding Fourier spectrum are shown in Figures 6(a) and 6(b), respectively. The spectrum shows significant responses at 85, 870 and 2,435 Hz, even though responses from lower modes are also present. A typical time-history of the base moment and the corresponding power density spectrum are shown in Figures 7(a) and 7(b), respectively. Although there is power spectral density at the fundamental frequency of 12 Hz, most structural response is associated with 85 Hz. There is also minor response at 870 Hz. Equipment fragility may be defined in terms of displacement, shear, moment, or strains at some

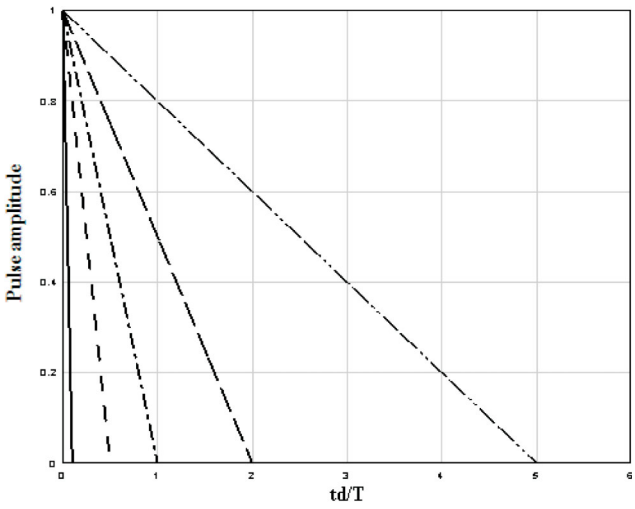

Figure 4. Base acceleration pulses.

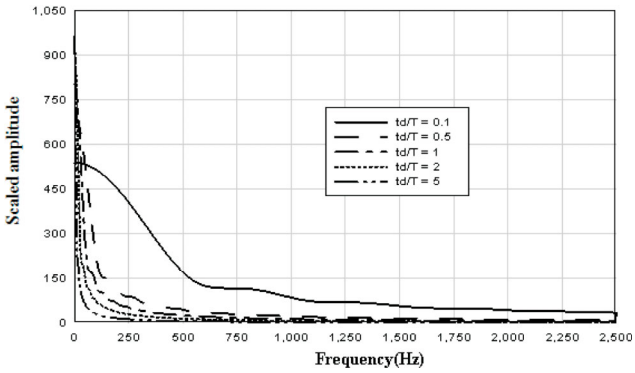

Figure 5. Frequency contents of the triangular pulses.

Table 3. Effect of pulse duration on structural response

t_d/T	Tip displacement (in.)	Base shear (lb)	Base moment (ft-lb)
0.1	0.11	54	101
0.5	0.31	118	263
1	0.36	137	304
2	0.38	146	325
5	0.40	152	338

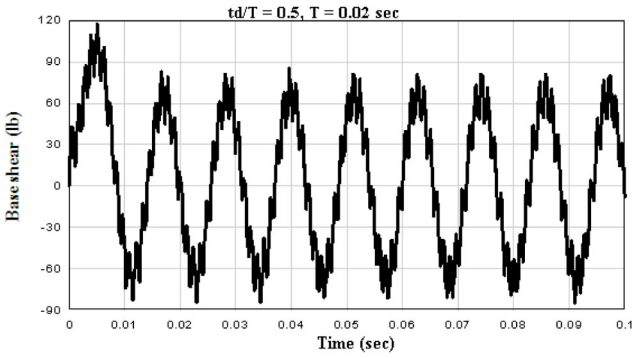

Figure 6(a). Base shear time-history for $t_d/T = 0.5$.

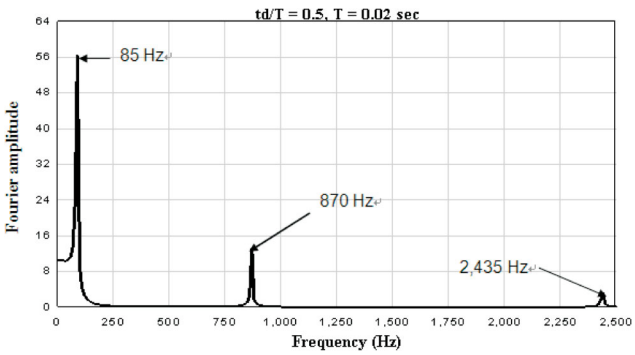

Figure 6(b). Fourier spectrum of base shear time-history for $t_d/T = 0.5$.

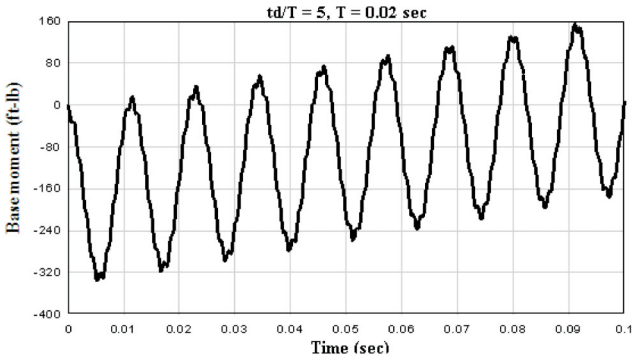

Figure 7(a). Base moment time-history for $t_d/T = 5$.

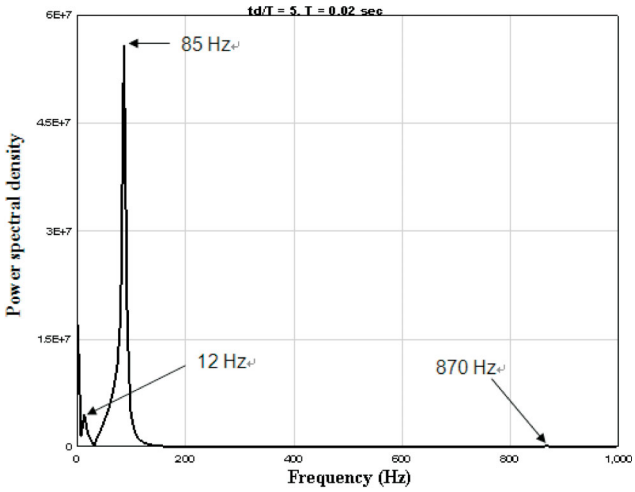

Figure 7(b). Power spectrum of base moment time-history for $t_d/T = 5$.

specified locations on the equipment. The base acceleration pulse amplitude can be adjusted until the fragility criteria are met. The fragility spectrum can subsequently be established. The fragility spectrum would thus depend upon the base acceleration pulse duration.

This example illustrates that a short duration base acceleration pulse can excite multiple modes in a piece of equipment. Assuming that the total response of the equipment is predominantly in the first mode is erroneous. The error induced from using a SDOF model such as in the shock response spectrum approach could be very significant.

6. Conclusions

This study points out the shortcomings of the SRS approach to characterizing equipment shock fragility:

(1) It was proven that SRS-based fragility spectra are not unique. Even for an equipment item which can be modeled by a simple SDOF undamped oscillator, different base excitations generally produce different fragility spectra.

(2) A cantilever beam model was used to show that the maximum repsonse may not always be at the fundamental frequency of the equipment.

In conclusion, this study has proven the inadequacy of the shock response spectrum for characterizing the shock fragility of equipment. Complex, nonlinear mechanical equipment subjected to multidirectional support motion is often not adequately represented by an SDOF model. Based on the results of this study, a more rigorous approach for assessing equipment fragility is required. The following points should be taken into account while conducting equipment fragility testing:

(1) When an equipment item is tested to determine its shock fragility, the test input waveform must be representative of the anticipated threat. Multidirectional support motion must be reproduced. Equipment tests should excite multiple response modes and produce the same failure modes, as the actual in-service base motion.

(2) Analytical equipment models must be detailed enough to reproduce the salient features of the actual equipment response. The model need not encompass the entire item of equipment, but it must adequately represent the critical components. The input motion used for analysis must mimic the in-service motion.

References

[1] Pan, Y., Agrawal, A. K. and Ghosn, M., "Seismic Fragility of Continuous Steel Highway Bridges in New York State," *Journal of Bridge Engineering*, Vol. 12, No. 6, pp. 689–699 (2007). doi: 10.1061/(ASCE)1084-0702(2007)12:6(689)

[2] Zhong, J. S., Gardoni, P., Rosowsky, D. and Haukaas, T., "Probabilistic Seismic Demand Models and Fragility Estimates for Reinforced Concrete Bridges with Two-Column Bents," *Journal of Engineering Mechanics*, Vol. 134, No. 6, pp. 495–504 (2008). doi: 10.1061/(ASCE)0733-9399(2008)134:6(495)

[3] Liang, C.-C., Yang, M.-F. and Tai, Y.-S., "Prediction of Shock Response for a Quadrupod-Mast Using Response Spectrum Analysis Method," *Ocean Engineering*, Vol. 29, No. 8, pp. 887–914 (2002).

[4] Shattarat, N. K., Symans, M. D., McLean, D. I. and Cofer, W. F., "Evaluation of Nonlinear Static Analysis Methods and Software Tools for Seismic Analysis of

Highway Bridges," *Engineering Structures*, Vol. 30, No. 5, pp. 1335–1345 (2008). doi: 10.1016/j.engstruct.2007.07.021

[5] Nielson, B. G. and DesRoches, R., "Seismic Fragility Methodology for Highway Bridges," *Structural Engineering and Public Safety*, Proceedings of the 2006 Structures Congress, May 18-21, St Louis, Missouri, pp. 1–9 (2006). doi: 10.1061/40889(201)174

[6] Yang, C. S., DesRoches, R. and Padgett, J. E., "Analytical Fragility Models for Box Girder Bridges with and without Protective Systems," *Proceedings of the 2009 Structures Congress*, Austin, Texas (2009). doi: 10.1061/41031(341)151

[7] Kim, S. H. and Shinozuka, M., "Fragility Curves for Concrete Bridges Retrofitted by Column Jacketing and Restrainers," *Proceedings of 6th U.S. Conference and Workshop on Lifeline Earthquake Engineering*, Long Beach, California (2003). doi: 10.1061/40687(2003)92

[8] Porter, K., Hamburger, R. and Kennedy, R., "Practical Development and Application of Fragility Functions," *Proceedings of the 2007 Structures Congress*, Long Beach, California (2007). doi: 10.1061/40944(249)23

[9] Zhang, J. and Huo, Y., "Fragility Function of Base Isolated Highway Bridges," *Proceedings of 18th Analysis and Computation Specialty Conference*, Vancouver, BC, Canada, pp. 1–17 (2008). doi: 10.1061/40944(249)23

[10] Chaudhuri, S. R. and Hutchinson, T. C., "Fragility of Bench-Mounted Equipment Considering Uncertain Parameters," *Journal of Structural Engineering*, Vol. 132, No. 6, pp. 884–898 (2006). doi: 10.1061/(ASCE)0733-9445(2006)132:6(884)

[11] Wilcoski, J., Gambill, J. B. and Smith, S. J., *The CERL Equipment Fragility and Protection Procedure (CEFAPP)*, Experimental Definition of Equipment Vulnerability to Transient Support Motions, US Army Corps of Engineers Construction Engineering Research Laboratories, USACERL Technical Report 97/58, March, p. 140 (1997).

[12] Dastous, J. B. and Filiatrault, A., "Seismic Displacement at Interconnection Points of Substation Equipment," *Proceedings of 6th U.S. Conference and Workshop on Lifeline Earthquake Engineering*, Long Beach, California (2003). doi: 10.1061/40687(2003)61

[13] Straub, D. and Der Kiureghian, A., "Improved Seismic Fragility Modeling from Empirical Data," *Structural Safety*, Vol. 30, No. 4, pp. 320–336 (2008). doi: 10.1016/j.strusafe.2007.05.004

[14] Zhu, Z. Y. and Soong, T. T., "Toppling Fragility of Unrestrained Equipment," *Earthquake Spectra*, Vol. 14, No. 4, pp. 695–712. doi: 10.1193/1.1586023

[15] Safford, F. B. and Tuttle, R. J., "Transient Shock Fragility and Hardness Assessment of Commercial Communications Equipment," *SAE International, Document No.740801*, February (1974). doi: 10.1016/0022-460X(89)90742-6

[16] Cunniff, P. F. and O'Hara, G. J., "A Procedure for Generating Shock Design Values," *Journal of Sound and Vibration*, October, Vol. 134, No. 1, pp. 155–164 (1989). doi: 10.1016/0022-460X(89)90742-6

[17] Salmonte, A. J., "Evaluation of Secondary and Higher Order Response Facets in Response Spectrum Analysis," *Nuclear Engineering and Design*, November, Vol. 109, No. 3, pp. 433–454 (1988). doi: 10.1016/0029-5493(88)90288-9

[18] Merkle, D. H, Rochefort, M. A. and Tuan, C. Y., "Equipment Shock Tolerance," *Final Report, ESL-TR-92-65*, U.S. Air Force Civil Engineering Support Agency, Tyndall Air Force Base, FL, April, p. 63 (1993).

[19] Coomes, J. R. and Roberts, W. B., "Report of Test on BUZZER, TYPE A-3 Submitted by Navy Yard, Portsmouth, N. H.," *Naval Research Laboratory*, Washington, DC, NRL-1396, p. 10 (1937).

[20] Kiger, S. A., Balsara, J. P. and Baylot, J. T., "A Computational Procedure for Peak In-structure Motions and Shock Spectra for Conventional Weapons," *The Shock and Vibration Bulletin* No. 54, Part 2, June, pp. 223–226 (1984).

Manuscript Received: Dec. 26, 2012
Accepted: Apr. 12, 2013